Atherosclerotic geometries exacerbate pathological thrombus formation poststenosis in a von Willebrand factor-dependent manner

Atherosclerotic geometries exacerbate pathological thrombus formation poststenosis in a von Willebrand factor-dependent manner

Erik Westein[a,b,1,2], Andries D. van der Meer[c,1], Marijke J. E. Kuijpers[a], Jean-Philippe Frimat[c], Albert van den Berg[c], and Johan W. M. Heemskerk[a,2]

[a]Department of Biochemistry, Cardiovascular Research Institute Maastricht, Maastricht University, 6200 MD Maastricht, The Netherlands; [b]Department of Atherothrombosis and Vascular Biology, Baker International Diabetes Institute, Heart and Diabetes Institute, Melbourne, Victoria 8008, Australia; and [c]BIOS/Lab on a Chip Group, MESA+ Institute for Nanotechnology, University of Twente, 7500 AE Enschede, The Netherlands

Edited by David A. Weitz, Harvard University, Cambridge, MA, and approved December 5, 2012 (received for review June 11, 2012)

Rupture of a vulnerable atherosclerotic plaque causes thrombus formation and precipitates cardiovascular diseases. In addition to the thrombogenic content of a plaque, also the hemodynamic microenvironment plays a major role in thrombus formation. How the altered hemodynamics around a plaque promote pathological thrombus formation is not well understood. In this study, we provide evidence that plaque geometries result in fluid mechanical conditions that promote platelet aggregation and thrombus formation by increased accumulation and activity of von Willebrand factor (vWF) at poststenotic sites. Resonant-scanning multiphoton microscopy revealed that in vivo arterial stenosis of a damaged carotid artery markedly increased platelet aggregate formation in the stenotic outlet region. Complementary in vitro studies using microfluidic stenotic chambers, designed to mimic the flow conditions in a stenotic artery, showed enhanced platelet aggregation in the stenotic outlet region at 60–80% channel occlusion over a range of input wall shear rates. The poststenotic thrombus formation was critically dependent on bloodborne vWF and autocrine platelet stimulation. In stenotic chambers containing endothelial cells, flow provoked increased endothelial vWF secretion in the stenotic outlet region, contributing to exacerbated platelet aggregation. Taken together, this study identifies a role for the shear-sensitive protein vWF in transducing hemodynamic forces that are present around a stenosis to a prothrombogenic microenvironment resulting in spatially confined and exacerbated platelet aggregation in the stenosis outlet region. The developed stenotic microfluidic chamber offers a realistic platform for in vitro evaluation of shear-dependent thrombus formation in the setting of atherosclerosis.

Atherosclerosis is characterized by progressive growth of atherosclerotic plaques in the arterial circulation. In an advanced stage of atherosclerosis, plaques will become stenotic and cause progressive obstruction of the arterial lumen. A current theorem is that rupture or erosion of a stenotic plaque is required for arterial thrombus formation and ensuing thrombotic complications, such as pulmonary embolism, myocardial infarction, or stroke (1). Better understanding of the precise regulation of thrombus formation in atherosclerotic vessel segments is critical for the improvement of current antithrombotic treatments.

Biochemical and hemodynamic factors contribute to thrombus formation at a vulnerable vessel wall (2–4). Thrombogenic components exposed upon plaque rupture—e.g. tissue factor, collagen and von Willebrand factor (vWF)—trigger initial activation of platelets and the coagulation system (5–7). Stable recruitment of platelets under flow to a growing thrombus involves vWF and fibrinogen as main ligands, which interact with glycoprotein (GP) Ib-V-IX and integrin $\alpha_{IIb}\beta_3$, respectively, as well as autocrine agonists produced by platelets themselves (8, 9). There is growing appreciation of the interplay of hemodynamics with this multireceptor process in plaque-containing areas (10). Intraluminal growth of a developing plaque, even in the absence of thrombus formation, will gradually alter the local blood flow dynamics (11). The flow disturbances at sites of severe stenosis may even lead to fatal occlusive thrombus formation in humans (12). Simulations indicate that plaque geometries induce gradients in pressure, flow velocity, and shear stress of the local blood flow, as a consequence of which autocrine agonists may get trapped that enhance platelet activation (13). However, the mechanisms dictating shear-dependent platelet aggregation at sites of atherosclerotic stenosis remain poorly understood.

In the present study, we used fast resonant-scanning multiphoton microscopy to investigate stenosis-dependent platelet aggregation in the murine carotid artery in vivo. In addition, we developed a microfluidic platform with stenotic flow channels to investigate platelet aggregation at defined positions relative to plaque-like geometries. Our data show that, both in vivo and in vitro, the shear stress conditions downstream of a stenotic site aggravate local platelet aggregation in a strongly vWF-dependent manner. This work highlights a central role for the shear-sensitive protein vWF in converting the fluid forces in the microenvironment downstream of a stenotic geometry into prothrombotic responses in a partly occluded artery.

Results

Exacerbation of Platelet Aggregation Poststenosis in Mouse Carotid Arteries in Vivo. The acute consequences of a vascular stenosis on platelet aggregation dynamics were investigated in vivo in the common carotid artery of C57BL/6 mice using fluorescence microscopy. Minor activation of the endothelium was applied through topical application of 12.5% (wt/vol) ferric chloride for a short period of 30 s to mimic the situation of moderate endothelial dysfunction as in the setting of atherosclerosis. This led to the formation of only small aggregates of fluorescently labeled platelets, which were scattered over the area affected by ferric chloride (Fig. 1*A*; 0–67 s). Subsequent induction of a stenosis by localized vessel compression with a 27-gauge needle to reach 80% lumen occlusion, markedly, resulted in an instantaneous growth response of aggregates in the stenosis outlet region, whereas the small aggregates in the stenosis inlet region remained unaffected (Fig. 1*B*, *Inset*). Overall, the stenotic vessel compression induced a greater than fourfold increase in thrombus size specifically in the stenosis outlet region (Fig. 1*B*).

Resonant-scanning multiphoton microscopy was used to determine the luminal thrombus composition inside the moving carotid artery at submicrometer resolution (*Methods*). Mice were

Author contributions: E.W. and A.D.v.d.M. designed research; E.W., A.D.v.d.M., M.J.E.K., and J.-P.F. performed research; E.W., A.D.v.d.M., J.-P.F., and A.v.d.B. contributed new reagents/analytic tools; E.W., A.D.v.d.M., J.-P.F., and A.v.d.B. analyzed data; and E.W., A.D.v.d.M., and J.W.M.H. wrote the paper.

The authors declare no conflict of interest.

This article is a PNAS Direct Submission.

[1]E.W. and A.D.v.d.M. contributed equally to this work.

[2]To whom correspondence may be addressed. E-mail: erik.westein@bakeridi.edu.au or jwm.heemskerk@maastrichtuniversity.nl.

This article contains supporting information online at www.pnas.org/lookup/suppl/doi:10.1073/pnas.1209905110/-/DCSupplemental.

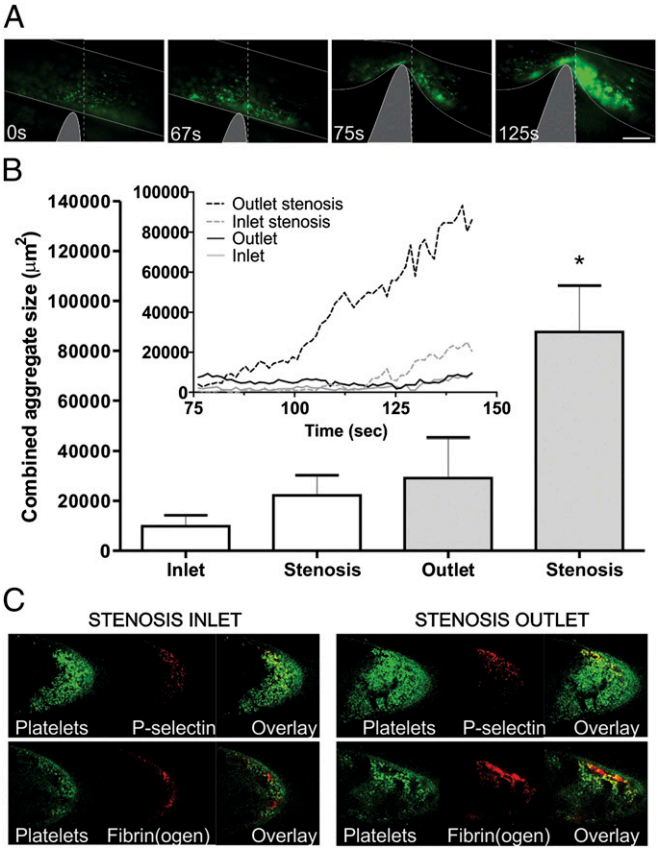

Fig. 1. Induced poststenotic thrombus formation in the murine carotid artery in vivo. Dissected mouse carotid arteries were subjected to brief (30 s) topical application of 12.5% (wt/vol) $FeCl_3$, and vessel stenosis was induced by a 27-gauge needle. In control experiments, no stenosis was induced. Intraluminal accumulation of fluorescence was monitored from preinjected CFSE-labeled mouse platelets using intravital fluorescence microscopy. (*A*) Wide-field fluorescence images showing thrombus formation downstream of stenosis site. The dotted lines (from bright-field images) indicate positions of vessel and needle; blood flow was from left to right. (Scale bar, 250 μm.) (*B*) Total aggregate size of fixed areas at regions of the stenosis inlet and outlet. *Inset* gives time plot of representative experiment. (*C*) Resonant scanning multiphoton fluorescence images during thrombus formation of preinjected labeled platelets (green), anti-P-selectin mAb (red), or fibrin (ogen) (red) in the stenotic inlet and outlet regions. In cross-sections, the carotid artery appears as an ellipse due to the angle between vessel and image focus plane (23°). Data are means ± SD; $n = 4$ (*$P < 0.05$).

preinjected with platelets labeled with carboxyfluorescein diacetate succinimidyl ester (CFSE) in combination with Alexa Fluor-labeled markers of platelet activation (labeled anti–P-selectin mAb or fibrinogen), and intraluminal thrombus formation was monitored in real time (Fig. 1*C*). The increased thrombus mass observed in the stenosis outlet section showed high staining for P-selectin that was associated with platelets close to the vessel wall. Furthermore, the thrombus in the stenosis outlet was enriched in fibrin(ogen) associated with the platelets. Jointly, these results demonstrate that stenosis of an injured artery exacerbates the thrombotic response immediately downstream of the stenosis.

Enhanced Platelet Aggregation Poststenosis in Microchannels in Vitro. To investigate how plaque geometries influence thrombus formation, an in vitro microfluidic platform was developed with multiple flow channels containing stenotic features of varying dimensions. Design was such that key rheological parameters were similar to those in the larger carotid arteries in humans (i.e., slopes of the stenosis, wall shear rates at the inlet and stenotic regions, and maximal flow elongation rate), while making advantage of the small fluid volumes needed for the microchannels (Table S1). We developed polydimethylsiloxane (PDMS) microchannels of 300 μm width, in which half-circular eccentric stenoses with a diameter of 600 or 1000 μm were present, i.e., two to three times the channel width (Fig. 2*A*). Lumen reductions varied from 20% to 80%, thus producing various degrees and slopes of stenosis. The microchannels were mounted on a pattern-coated coverslip, containing discrete patches (80 μm width) of immobilized vWF/fibrinogen, i.e., principal platelet-adhesive components in thrombus formation (Fig. 2*A* and Fig. S1*A*). Computational analysis indicated that the wall shear rate was symmetrically distributed over the stenosis artifact. At 80% stenosis, it was eightfold higher in the apex region than in the prestenotic segment (Fig. 2*B* and Fig. S1*B*). At an input wall shear rate of 1,000 s^{-1}, a platelet traveling through the stenosis thus experiences an increase in shear rate to 8,000 s^{-1}, followed by an identical decrease after the stenosis (Fig. S1*C*). These calculations are in agreement with experimental measurement of the velocity of flowing platelets at 2 μm from the channel bottom (Fig. S1*D*).

To investigate the effect of stenotic geometries on platelet activation, whole blood labeled with 3,3′-dihexyloxacarbocyanine iodide ($DiOC_6$) was perfused through the channels containing patches of vWF/fibrinogen. Upon perfusion at (arterial) input wall shear rate of 1,000 s^{-1}, aggregates formed of adhered platelets, predominantly in the stenosis outlet region, as indicated by a >2.5-fold increase in platelet deposition (Fig. 3*A*). In contrast, only single platelets adhered in the stenosis inlet region and in straight sections of the channel. Platelet aggregation in the stenosis outlet region was typically dependent on the degree of stenosis, being most prominent at 60–80% lumen reduction (Fig. 3*B* and Movie S1). Thrombus height ranged from single platelets

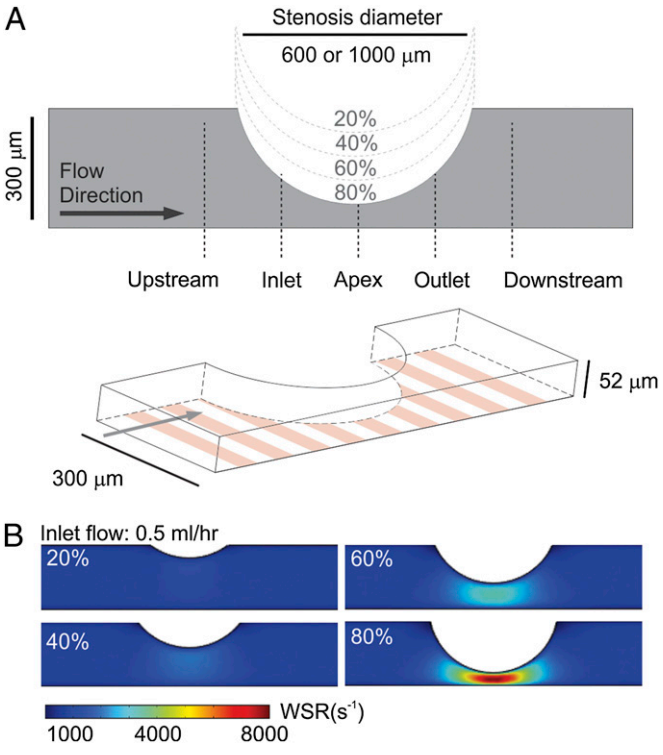

Fig. 2. Wall shear rate patterns in microfluidic PDMS channels with a stenotic shape. (*A*) Drawing of microchannel with width of 300 μm, eccentric circular stenotic indentation (600- or 1,000-μm Ø), and lumen restriction of 20–80%. The channel bottom contains discontinuous strips (80 μm) with immobilized vWF/fibrinogen. (*B*) Computational fluid dynamics analysis displaying the wall shear rate (WSR) near the channel bottom in a microchannel with 20–80% stenosis (600-μm Ø) at 1,000 s^{-1} inlet WSR (0.5 mL/h).

in the upstream and downstream regions to full channel height (52 μm) in the outlet region. The enhanced platelet aggregation in the stenosis outlet zone was present at inlet wall shear rates of 600, 1,000, and 2,000 s^{-1} (Fig. 3*C*), and was eliminated by pretreatment of the blood with blockers of GPIbα (6B4 mAb) or integrin $\alpha_{IIb}\beta_3$ (c7E3 mAb). Similarly, treatment of the blood with the platelet inhibitor, iloprost, prevented enhanced platelet aggregation in the stenosis outlet region (Fig. 3*C*). Suppressing the effects of autocrine mediators with ADP receptor blockers and indomethacin had a strong inhibitory effect on platelet aggregation in the stenosis outlet region (Fig. 3*C* and Fig. S2).

In control studies with straight channels, we found that blood perfusion up to a wall shear rate of 8,000 s^{-1} did not initiate platelet aggregation (Fig. S3*A*). However, anticoagulation of the blood with hirudin or D-phenylalanyl-L-prolyl-L-arginine chloromethyl ketone (PPACK), instead of citrate, also yielded platelet aggregation specifically in the stenotic outlet region (Fig. S3*B*). Detailed analysis of the platelet trajectories during flow indicated that this poststenotic platelet aggregation was not due to translocation of platelets from upstream to downstream patches, neither to lodging of upstream-formed platelet aggregates (Fig. S4 and Movie S1).

Key Role of Bloodborne vWF in Stenosis-Dependent Platelet Aggregation. Platelet adhesion under high shear conditions is critically dependent on vWF binding to GPIbα. To assess whether plasma vWF was a limiting factor in stenosis-dependent platelet aggregation, normal whole blood was supplemented with 20 μg/mL (2.0 IU/mL) purified vWF. This threefold increase in vWF concentration resulted in a corresponding increase in the magnitude of platelet aggregation in the stenosis outlet region (Fig. 4*A*, *Left*). No aggregation was observed in the straight sections of the flow channel. To confirm the importance of vWF, whole-blood samples were used from patients with dilutional coagulopathy treated with 1-desamino-8-D-arginine vasopressin (DDAVP) to increase plasma levels of vWF and factor VIII. The administration of DDAVP resulted in an overall 1.9-fold increase in aggregation response in the stenosis outlet region (Fig. 4*A*, *Center*). Again, upstream and downstream sections were not reactive. Furthermore, a reconstituted system was used with washed platelets and red blood cells. In this case, platelets did not aggregate in the absence of vWF but showed asymmetric aggregation in the stenosis outlet region after supplementation of 10 μg/mL vWF (Fig. 4*A*, *Right*). Confocal fluorescence microscopy after 4 min of platelet-depleted whole-blood perfusion revealed a significant increase in vWF staining in the stenotic region compared with upstream sections of the channel (Fig. 4*B*). Interestingly, applying the wall shear rates present in the stenosis outlet (~5,700 s^{-1}) and apex region (~8,000 s^{-1}) in straight channels did not increase vWF staining intensity.

At high shear conditions, binding of the vWF A1-domain to the GPIbα receptor induces a rise in cytosolic Ca^{2+}, and subsequent platelet activation (14). This was investigated with platelets, loaded with the Ca^{2+} probe, Fluo-4, and reconstituted in a medium with plasma and red blood cells [40% (vol/vol) hematocrit]. A larger fraction of surface-adherent platelets exhibited transient elevation in Ca^{2+} in the inlet and outlet zones of the stenosis, i.e., where the platelets were subjected to flow gradients (Fig. 4*C*). Blocking of GPIbα with 6B4 mAb eliminated the Ca^{2+} rises at both sites, thus confirming the role of this receptor in shear gradient-dependent platelet activation.

Enhanced Platelet Aggregation Poststenosis by Increased Endothelial Secretion of vWF. Platelet aggregation in vivo relies on both hematological parameters and vascular factors. To investigate this, microfluidic stenotic channels were used with endothelial cells, cultured to a confluent monolayer (Fig. 5*A*). These endothelial cells were subjected to buffer perfusion at a fluid wall shear rate of 1,000 s^{-1}. Markedly, cells that were located in the outlet region of the stenosis displayed a strong increase in surface-expressed vWF, such in contrast to cells at the stenosis inlet region. The vWF staining pattern indicated strings of vWF multimers in the outlet region (Fig. 5*A*, arrows). This is consistent with the finding from others, reporting that cultured endothelial cells can release

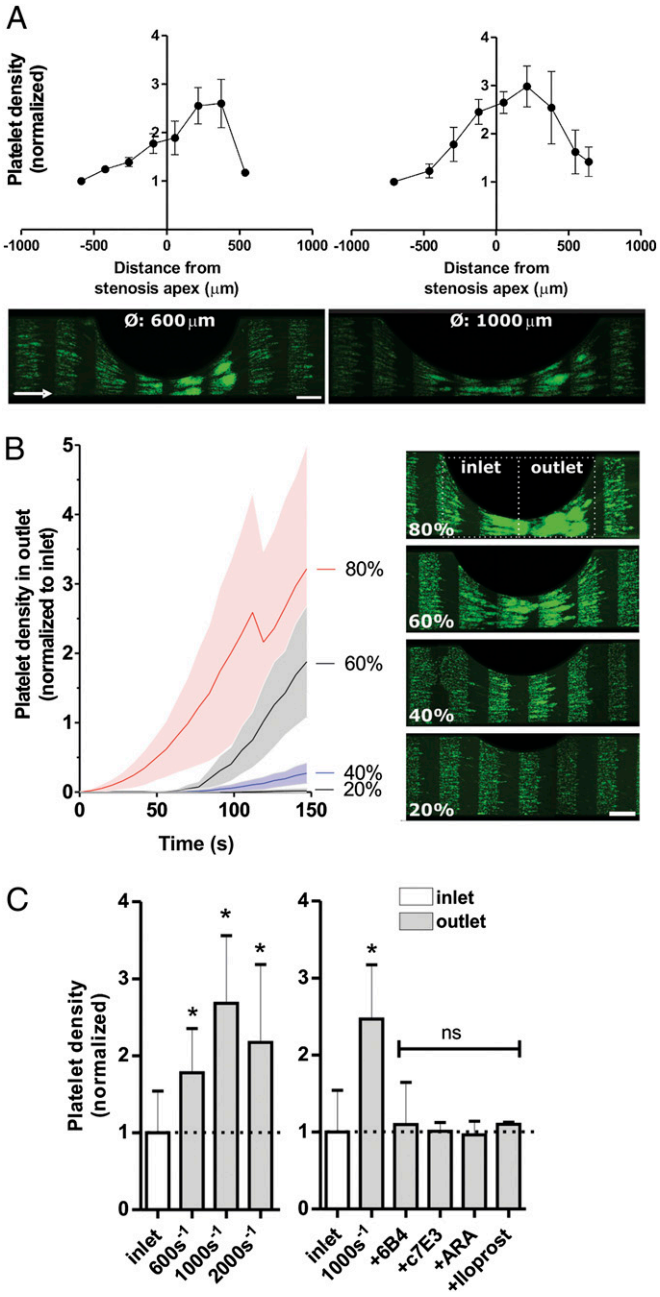

Fig. 3. Exacerbated platelet aggregation in microfluidic channels at stenosis outlet region. Platelets in whole blood were labeled with $DiOC_6$ and perfused through a stenotic microchannel (600- or 1,000-μm Ø and 20–80% stenosis) at input wall shear rate of 1,000 s^{-1}. (*A*) Platelet density at individual patches of vWF/fibrinogen around the stenosis apex normalized to values obtained on the first patch. Note that platelet aggregate formation is asymmetrically distributed toward the stenosis outlet region. (Scale bar, 100 μm.) (*B*) (*Left*) Mean platelet density in the stenosis outlet region at various degrees of stenosis (normalized to values of the first patch at the channel inlet). The sudden intensity reduction at 80% stenosis is due to an embolization event. (*Right*) Representative confocal fluorescence images of platelet aggregate formation at 20–80% stenosis at 120 s of blood flow. Note the single adhered platelets at patches of vWF/fibrinogen before and after the stenosis, and platelet aggregates in patches at the stenotic outlet region (60–80% stenosis). (Scale bar, 100 μm.) (*C*) Mean platelet density in the stenosis outlet region at various input wall shear rates and in the presence of inhibitors, 6B4 (anti-GPIbα mAb), c7E3 (anti-$\alpha_{IIb}\beta_3$ mAb), ARA (autocrine receptor antagonists: cangrelor at 30 μM, MRS2179 at 100 μM, indomethacin at 10 μM) or iloprost (prostacyclin analog, 55 nM). Data represent means ± SD; $n = 3$–4 (*$P < 0.05$).

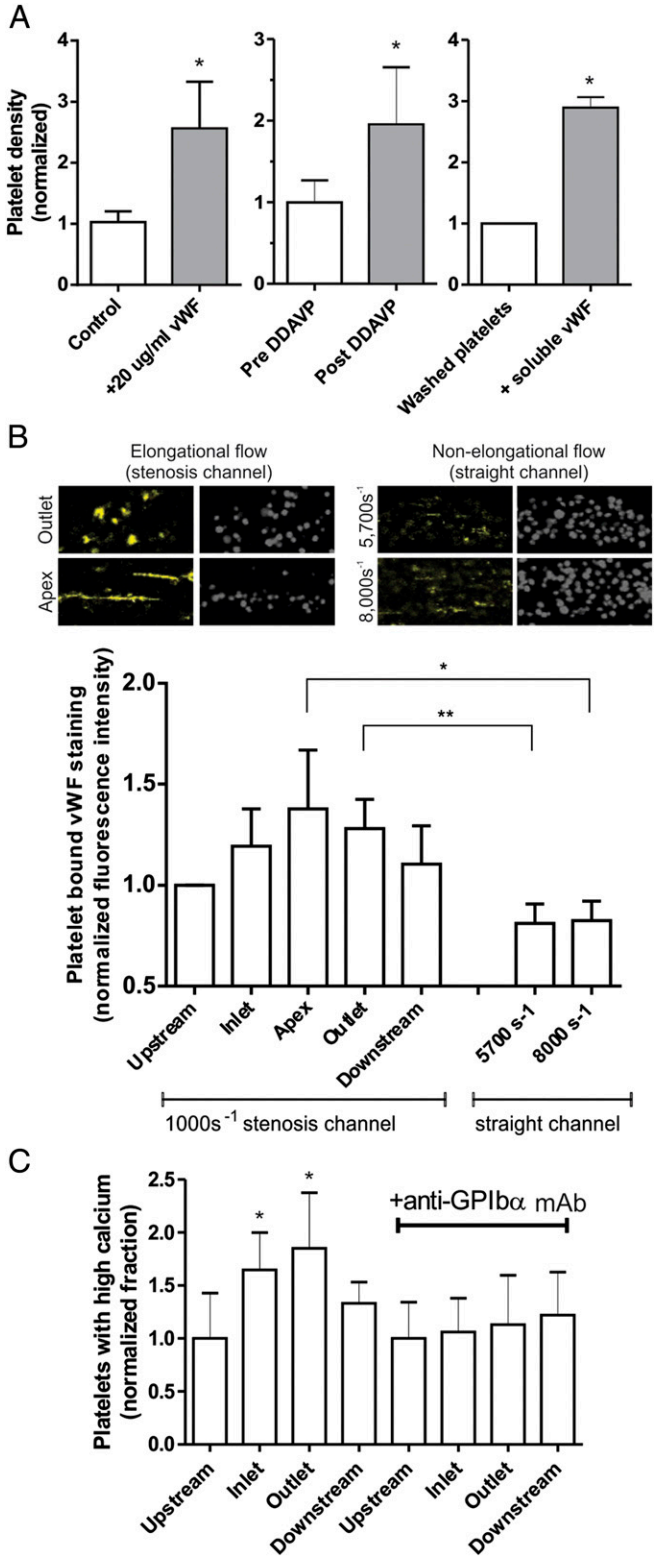

Fig. 4. Role of vWF in stenosis-induced platelet aggregation. (*A*) Platelet density in stenotic (600-μm Ø) outlet regions at input wall shear rate of 1,000 s^{-1}. Values are normalized against control condition (open bars). (*Left*) Control whole blood supplemented with 20 μg/mL vWF. (*Center*) Whole blood from patients with dilutional coagulopathy was monitored pretreatment and posttreatment with DDAVP. (*Right*) Effect of vWF addition (10 μg/mL) to 3×10^8/mL washed platelets, reconstituted with 40% (vol/vol) red blood cells. (*B*) Representative micrographs showing platelet-bound vWF (yellow) and platelets (grayscale) under conditions of elongational flow in the stenosis channels and nonelongational flow in straight channels. Platelet-depleted blood was perfused through the stenosis channels at 1,000 s^{-1} input wall shear or through the straight channels at 5,700 and 8,000 s^{-1} to represent wall shear rates present in the stenosis outlet and apex, respectively. (*Lower*) Fluorescence staining intensities of platelet-bound vWF at various positions relative to the stenosis normalized to values upstream. vWF staining intensity at the apex and outlet of the stenosis channels is increased compared with the straight channels. (*C*) Effect of GPIb blockage (20 μg/mL 6B4 mAb) on shear-induced Ca^{2+} responses of single, surface-adherent platelets. Shown are fractions of surface-adherent platelets displaying a Ca^{2+} response. Data are means ± SD; $n \geq 3$ (*$P < 0.05$, **$P < 0.01$).

multimeric vWF following histamine stimulation (15). Quantitative analysis after vWF staining showed that the shear-induced vWF multimers occupied a 15-fold higher surface area in the outlet region, compared with the inlet region (Fig. 5*B*). However, endothelial cells in channels not containing a stenosis failed to produce strings of vWF within the same time frame, up to shear rates of 8,000 s^{-1} (Fig. S3*C*).

Whole-blood perfusion through the endothelial-covered channels led to substantial platelet aggregation specifically in the stenotic outlet region (Fig. 5*C*). Platelet aggregates grew to large sizes (mean area, 13,474 μm^2), whereas platelet aggregates in the inlet region and further upstream regions remained only small (mean, 1,378 μm^2). In control experiments, the endothelial cells were stimulated with histamine, to provoke vWF release before blood perfusion. In this case, large-size platelet aggregates (mean size, 6,496 μm^2) were formed throughout the channel, hence also in the straight upstream sections (Fig. 5*D*). These results reveal compound effects of the hemodynamic shear stress in stenosis outlet regions, which stimulate endothelial vWF secretion, and vWF-dependent platelet aggregation, both facilitating pathological thrombus formation.

Discussion

In this study we demonstrate both in vivo and in vitro—using engineered stenotic microfluidic channels—that thrombus formation is exacerbated at sites downstream of stenotic atherosclerotic plaque geometries. Increased platelet aggregation in the stenotic outlet region strongly relies on plasma and endothelial vWF, which causes spatially confined platelet activation (Fig. 6). These findings shed light on the process of atherothrombosis in that the stenotic geometry of a plaque, and the consequently altered blood flow pattern, appears to be an important regulatory factor of platelet aggregation and thrombus formation. Thus, plaque rupture sites in vessel segments immediately downstream of a stenosis may be at increased risk of triggering thrombus formation.

The phenomenon that shear rate gradients can influence thrombus formation has recently been described (16). Microshear gradients surrounding a thrombus recruit platelets in a downstream direction. Such clot asymmetry is also observed in the laser injury model of thrombosis in mice (17). The present data significantly extend this work in demonstrating the importance of vWF acting as a regulator of platelet aggregation at poststenotic sites with decreasing wall shear rate. Platelet aggregation at poststenotic sites appears to be strictly dependent on the release of platelet agonists and, hence, is fundamentally different from the mechanism of microshear gradient-dependent platelet aggregation, earlier described by Nesbitt et al. (16). Already in the 1970s, it was suggested that alterations in blood flow dynamics around atherosclerotic plaques link to occlusive thrombus formation (12), and that mild vascular damage in the presence of lumen reduction has thrombotic consequences, such as in the classical Foltz model of thromboembolism (18). Fluid dynamic studies from the 1990s reported that stenotic regions influenced platelet aggregation by way of flow perturbations and recirculation zones (19, 20). In particular, collagen ligands in combination with extremely high shear rates were used to detect poststenotic aggregate formation (21, 22). However, in the present study, the flow conditions in the microfluidics channel were

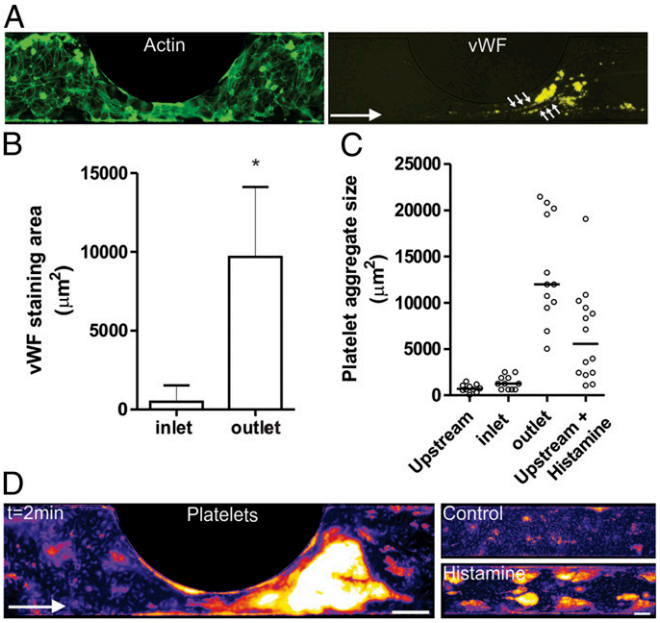

Fig. 5. Poststenotic vWF secretion enhances platelet aggregation in microchannels covered with endothelial cells. Confluent HUVECs in stenotic microchannels were perfused with buffer or whole blood at an input wall shear rate of 1,000 s^{-1}. (*A*) (*Left*) Staining for cytoskeletal actin with FITC-conjugated phalloidin. (*Right*) Staining for surface-expressed vWF in the stenosis outlet region after 1 min buffer perfusion. (*B*) Quantification of vWF staining in stenosis inlet and outlet regions. (*C*) Platelet aggregate size after whole-blood perfusion (1,000 s^{-1}) at indicated locations relative to the stenosis. (*D*) Confocal images of platelet aggregates formed on endothelial cells after whole-blood perfusion. Platelets were labeled with $DiOC_6$ (displayed with false color). Prior endothelial stimulation with histamine (500 μM), causing aggregate formation in all channel sections. (Scale bars, 100 μm.) Data are means ± SD; $n = 3–4$ (*$P < 0.05$).

purposely kept laminar, while vWF and fibrinogen were chosen as adhesive ligands that best represent the surface of growing thrombi. Under these conditions, we found that the combination of weakly platelet-activating vWF/fibrinogen plus shear alterations at a stenosis outlet is sufficient for a strong proaggregatory effect.

A useful measure for the variable wall shear rate to which platelets are exposed is the integral shear history, i.e., the product of shear rate and exposure time (23). A reported threshold of the integral shear history for platelet aggregation in response to constant shear is 50 Pa·s (24). In our study, the integral shear history is <0.054 Pa·s; hence the platelet-activating effect of the stenosis must be caused by additional factors other than the short exposure to high shear stress.

Rises in cytosolic Ca^{2+} are required for full platelet activation, e.g., by causing release of autocrine mediators (25). We found that plasma vWF adhesion to surface-adherent platelets in the inlet and outlet regions of a stenosis triggers GPIbα-dependent Ca^{2+} signaling, potentially by more easy unfolding of the adhered vWF under conditions of elongational flow compared with constant flow (26). Indeed, the binding of vWF to platelets was increased only under elongational flow conditions, not constant flow, and led to a symmetric distribution of vWF binding throughout the high shear region of the stenosis. We could calculate that the elongational shear rate was maximal in the inlet of the stenotic channels, and displayed similar values for a stenosis in a carotid artery in humans and the in vivo mouse model (Fig. S5 *A–C*). Although the symmetrical distribution of enhanced vWF deposition is consistent with the symmetrical distribution of Ca^{2+} signaling in surface-adherent platelets, it is in apparent contradiction with the asymmetric (i.e., downstream) platelet aggregation. Thrombus formation was maximum immediately downstream of the stenosis apex and did not extend beyond the stenotic feature, which is consistent with mathematical simulations showing that local concentration profiles of autocrine agonists rapidly decline due to diffusion effects (27). Indeed, thrombus formation in the outlet region was eliminated in the presence of cyclooxygenase inhibition and ADP receptor blockade. The high shear stress in the stenosis apex may trigger release of thromboxane A_2 and ADP, which are known to contribute to aggregate formation at high shear stress (28, 29), whereas the immediate reduction in shear stress load in the outlet region favors autocrine agonist-dependent platelet aggregation. The stenotic geometry couples high shear stress-induced release of autocrine agonists with a region of low shear stress. This coupling mechanism is not present in nonstenotic channels and, as expected, did not induce overt aggregate formation even under pathological shear rates (8,000 s^{-1}). However, in a straight channel, the coupling mechanism has essentially been demonstrated by Neeves et al. (30) who artificially introduced high levels of ADP at a site of platelet adhesion to fibrinogen under low shear rate (250 s^{-1}) and observed overt platelet aggregation. The previously described process of activation-independent platelet aggregation (31) may well play a role in the stenosis apex, which in combination with the coupling to a low shear zone exacerbates platelet aggregation.

Endothelial cells may further contribute to stenosis-induced platelet aggregation by enhanced vWF secretion and accumulation in the stenotic outlet region (Fig. 6). This is consistent with observations that endothelial cells undergo flow-induced activation (32), leading to vWF secretion from Weibel–Palade bodies (33), and that vWF is a critical mediator of thrombus formation under conditions of near-vascular occlusion (34). The current data of geometry-dependent platelet aggregation in the poststenosis region are compatible with evidence that mural thrombi are preferentially formed in the downstream direction, once a semiocclusive atherosclerotic plaque ruptures or denudates. Also, arteriograms show that plaque growth after episodes of thrombosis occurs preferentially in the downstream direction (35, 36). Furthermore, endothelial cells located in the downstream side of plaques have been shown to be apoptotic (37), procoagulant (38), and adhesive to nonactivated platelets (39). There is also evidence that the geometry of the downstream side of plaques is linked to vulnerability to rupture. Culprit lesions compared with nonculprit lesions were

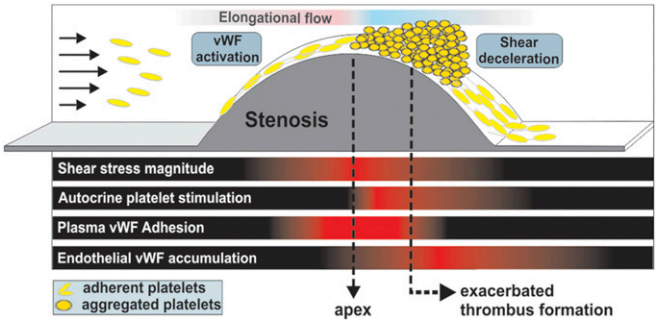

Fig. 6. Atherosclerotic geometries exacerbate pathological thrombus formation poststenosis in a vWF-dependent manner. Platelet aggregation at sites immediately downstream of vascular stenosis is promoted by multiple spatially confined variables (indicated arbitrarily by the red scale bar). The stenotic geometry induces a symmetrically distributed shear stress magnitude, being highest at the stenosis apex. Autocrine agonists are released from platelets that pass through the high shear stress region of the stenosis apex. Subsequent autocrine platelet stimulation is maximum immediately downstream of the apex and diminishes rapidly due to dilutional effects of the autocrine agonists. Elongational flow in the stenosis inlet activates plasma vWF and leads to symmetrically distributed vWF adhesion to adherent platelets. The symmetric shear stress effects on the endothelium result in increased vWF secretion from endothelial cells in the stenosis outlet region. Taken together, the outlet region of stenotic geometries exacerbate thrombus formation through spatially confining (*i*) increased levels of vWF content, (*ii*) autocrine platelet stimulation, and (*iii*) shear deceleration.

found to have a higher outflow angle with a maximum of 36.6° (40), which closely resembles the outflow angle of 39° in our study.

In conclusion, we identified a central role for the shear-sensitive protein vWF in promoting platelet aggregation at post-stenotic sites with a negative shear rate gradient. This argues for the monitoring of atherosclerotic plaque geometries and comparing these with local endothelial vWF release and plasma levels of vWF, in predicting the risk of atherothrombosis.

Methods

For further details, see *SI Methods*.

In Vivo Stenosis Model. All experiments were approved by the Maastricht University animal experimental and care committees. Carotid arteries of C57BL/6 mice were carefully dissected free from surrounding tissue. Mice were then injected i.v. with CFSE-labeled platelets, obtained from a donor mouse (8), and with Alexa Fluor (AF)-546–labeled fibrinogen or AF-568 anti-CD62P mAb, as appropriate. Mild vessel damage was induced by topical application of 12.5% (wt/vol) ferric chloride for 30 s. Local stenosis was achieved by indentation of the carotid wall with a 27-gauge needle controlled by a micromanipulator. Thrombus formation was monitored by resonant-scanning multiphoton microscopy (Leica SP5 system). This technique combines the deep penetration of two-photon microscopy (0.8 mm at 800-nm excitation) with a fast scanning rate (effective 25 frames/s) using the resonant-scanning module, thus allowing high-quality recording of confocal images from an intraluminal thrombus of a moving carotid artery.

In Vitro Stenosis Models. Microfluidic chips were poured from PDMS, using a mold with a series of parallel microchannels (300-μm width, 52-μm height) each with a one-sided stenosis of 20%, 40%, 60%, or 80% lumen reduction. A micropattern with strips of immobilized vWF/fibrinogen was generated by coating a glass coverslip with a mixture of vWF (20 μg/mL) and fibrinogen (50 μg/mL) in Hepes buffer, pH 7.45 (134 mM NaCl, 20 mM Hepes, 12 mM $NaHCO_3$, 2.9 mM KCl, 1 mM $MgCl_2$, 0.34 mM Na_2HPO_4, 5 mM glucose), using a separate meandering microfluidic channel (80-μm width). The PMDS microchannel chip was then placed on the coverslip. Whole human blood [anticoagulated with 3.8% (wt/vol) sodium citrate, hirudin, or PPACK] was perfused through the microchannels at 1,000 s^{-1} input wall shear rate, unless otherwise stated. Blood samples were preincubated with $DiOC_6$ (2 μg/mL) and/or platelet antagonists before perfusion. Fast recording of confocal images was done with a LSM Live-7 line-scanning system (Zeiss) operating at 50 Hz.

Endothelial Cell-Covered Microchannels. Human umbilical vascular endothelial cells (HUVECs) (20×10^6 cells/mL) were seeded into stenotic microchannels precoated with fibronectin (2 mg/mL), and grown overnight to confluency under 5% CO_2 atmosphere at 37 °C. Channels containing endothelial cells were perfused with human blood or EBM-2 medium (37 °C), and stained for release of vWF using mouse anti-vWF monoclonal antibody (1:100) and FITC-labeled goat anti-mouse IgG (1:100), added to the perfusion medium (no fixation). Surface expression of vWF was visualized in real time by fluorescence microscopy.

ACKNOWLEDGMENTS. We thank Dr. H. Deckmyn for providing anti-GPIb mAb, Dr. B. de Laat for purified vWF, L. de Vreede for production of SU-8 master molds, Dr. M. van Zandvoort and T. Rademakers for technical assistance with multiphoton experiments, and Dr. K. Peter for access to experimental tools and infrastructure. E.W. holds Australian National Health and Medical Research Council Overseas Training Fellowship ID 606742. This work was supported by the Cardiovascular Centre (Maastricht University Medical Center, Maastricht, The Netherlands); the Centre for Translational Molecular Medicine, Innovative Coagulation Diagnostics (INCOAG) (The Netherlands); The Netherlands Organization for Scientific Research Nanotox Chip Project 11521; and the European Research Council eLab$_4$life Project.

1. Burke AP, et al. (2001) Healed plaque ruptures and sudden coronary death: Evidence that subclinical rupture has a role in plaque progression. *Circulation* 103(7):934–940.
2. Jackson SP (2007) The growing complexity of platelet aggregation. *Blood* 109(12): 5087–5095.
3. Munnix IC, Cosemans JM, Auger JM, Heemskerk JW (2009) Platelet response heterogeneity in thrombus formation. *Thromb Haemost* 102(6):1149–1156.
4. Furie B, Furie BC (2005) Thrombus formation in vivo. *J Clin Invest* 115(12):3355–3362.
5. Siess W, et al. (1999) Lysophosphatidic acid mediates the rapid activation of platelets and endothelial cells by mildly oxidized low density lipoprotein and accumulates in human atherosclerotic lesions. *Proc Natl Acad Sci USA* 96(12):6931–6936.
6. Cosemans JM, et al. (2005) Contribution of platelet glycoprotein VI to the thrombogenic effect of collagens in fibrous atherosclerotic lesions. *Atherosclerosis* 181(1):19–27.
7. Reininger AJ, et al. (2010) A 2-step mechanism of arterial thrombus formation induced by human atherosclerotic plaques. *J Am Coll Cardiol* 55(11):1147–1158.
8. Kuijpers MJ, et al. (2009) Complementary roles of platelets and coagulation in thrombus formation on plaques acutely ruptured by targeted ultrasound treatment: A novel intravital model. *J Thromb Haemost* 7(1):152–161.
9. Nieswandt B, Watson SP (2003) Platelet-collagen interaction: Is GPVI the central receptor? *Blood* 102(2):449–461.
10. Nesbitt WS, Mangin P, Salem HH, Jackson SP (2006) The impact of blood rheology on the molecular and cellular events underlying arterial thrombosis. *J Mol Med (Berl)* 84(12):989–995.
11. Hyun S, Kleinstreuer C, Archie JP, Jr. (2000) Hemodynamics analyses of arterial expansions with implications to thrombosis and restenosis. *Med Eng Phys* 22(1):13–27.
12. Charles RG, Epstein EJ (1983) Diagnosis of coronary embolism: A review. *J R Soc Med* 76(10):863–869.
13. Folie BJ, McIntire LV (1989) Mathematical analysis of mural thrombogenesis. Concentration profiles of platelet-activating agents and effects of viscous shear flow. *Biophys J* 56(6):1121–1141.
14. Chow TW, Hellums JD, Moake JL, Kroll MH (1992) Shear stress-induced von Willebrand factor binding to platelet glycoprotein Ib initiates calcium influx associated with aggregation. *Blood* 80(1):113–120.
15. Dong JF, et al. (2002) ADAMTS-13 rapidly cleaves newly secreted ultralarge von Willebrand factor multimers on the endothelial surface under flowing conditions. *Blood* 100(12):4033–4039.
16. Nesbitt WS, et al. (2009) A shear gradient-dependent platelet aggregation mechanism drives thrombus formation. *Nat Med* 15(6):665–673.
17. Falati S, Gross P, Merrill-Skoloff G, Furie BC, Furie B (2002) Real-time in vivo imaging of platelets, tissue factor and fibrin during arterial thrombus formation in the mouse. *Nat Med* 8(10):1175–1181.
18. Folts JD, Crowell EB, Jr., Rowe GG (1976) Platelet aggregation in partially obstructed vessels and its elimination with aspirin. *Circulation* 54(3):365–370.
19. Schoephoerster RT, Oynes F, Nunez G, Kapadvanjwala M, Dewanjee MK (1993) Effects of local geometry and fluid dynamics on regional platelet deposition on artificial surfaces. *Arterioscler Thromb* 13(12):1806–1813.
20. Bluestein D, Niu L, Schoephoerster RT, Dewanjee MK (1997) Fluid mechanics of arterial stenosis: Relationship to the development of mural thrombus. *Ann Biomed Eng* 25(2):344–356.
21. Wootton DM, Markou CP, Hanson SR, Ku DN (2001) A mechanistic model of acute platelet accumulation in thrombogenic stenoses. *Ann Biomed Eng* 29(4):321–329.
22. Barstad RM, Roald HE, Cui Y, Turitto VT, Sakariassen KS (1994) A perfusion chamber developed to investigate thrombus formation and shear profiles in flowing native human blood at the apex of well-defined stenoses. *Arterioscler Thromb* 14(12):1984–1991.
23. Zhang JN, et al. (2003) Duration of exposure to high fluid shear stress is critical in shear-induced platelet activation-aggregation. *Thromb Haemost* 90(4):672–678.
24. Sheriff J, Bluestein D, Girdhar G, Jesty J (2010) High-shear stress sensitizes platelets to subsequent low-shear conditions. *Ann Biomed Eng* 38(4):1442–1450.
25. Heemskerk JW, Bevers EM, Lindhout T (2002) Platelet activation and blood coagulation. *Thromb Haemost* 88(2):186–193.
26. Sing CE, Alexander-Katz A (2010) Elongational flow induces the unfolding of von Willebrand factor at physiological flow rates. *Biophys J* 98(9):L35–L37.
27. Hubbell JA, McIntire LV (1986) Platelet active concentration profiles near growing thrombi. A mathematical consideration. *Biophys J* 50(5):937–945.
28. Lecut C, et al. (2004) Principal role of glycoprotein VI in alpha2beta1 and alphaIIbbeta3 activation during collagen-induced thrombus formation. *Arterioscler Thromb Vasc Biol* 24(9):1727–1733.
29. Nesbitt WS, et al. (2003) Intercellular calcium communication regulates platelet aggregation and thrombus growth. *J Cell Biol* 160(7):1151–1161.
30. Neeves KB, Diamond SL (2008) A membrane-based microfluidic device for controlling the flux of platelet agonists into flowing blood. *Lab Chip* 8(5):701–709.
31. Ruggeri ZM, Orje JN, Habermann R, Federici AB, Reininger AJ (2006) Activation-independent platelet adhesion and aggregation under elevated shear stress. *Blood* 108(6):1903–1910.
32. Galbusera M, et al. (1997) Fluid shear stress modulates von Willebrand factor release from human vascular endothelium. *Blood* 90(4):1558–1564.
33. Sun RJ, Muller S, Wang X, Zhuang FY, Stoltz JF (2000) Regulation of von willebrand factor of human endothelial cells exposed to laminar flows: An in vitro study. *Clin Hemorheol Microcirc* 23(1):1–11.
34. Ni H, et al. (2000) Persistence of platelet thrombus formation in arterioles of mice lacking both von Willebrand factor and fibrinogen. *J Clin Invest* 106(3):385–392.
35. Yokoya K, et al. (1999) Process of progression of coronary artery lesions from mild or moderate stenosis to moderate or severe stenosis: A study based on four serial coronary arteriograms per year. *Circulation* 100(9):903–909.
36. Smedby O (1997) Do plaques grow upstream or downstream?: An angiographic study in the femoral artery. *Arterioscler Thromb Vasc Biol* 17(5):912–918.
37. Tricot O, et al. (2000) Relation between endothelial cell apoptosis and blood flow direction in human atherosclerotic plaques. *Circulation* 101(21):2450–2453.
38. Bombeli T, Karsan A, Tait JF, Harlan JM (1997) Apoptotic vascular endothelial cells become procoagulant. *Blood* 89(7):2429–2442.
39. Bombeli T, Schwartz BR, Harlan JM (1999) Endothelial cells undergoing apoptosis become proadhesive for nonactivated platelets. *Blood* 93(11):3831–3838.
40. Ledru F, et al. (1999) Geometric features of coronary artery lesions favoring acute occlusion and myocardial infarction: A quantitative angiographic study. *J Am Coll Cardiol* 33(5): 1353–1361.